applied sciences

MDPI

Article

Numerical Study and Geometric Investigation of the Influence of Rectangular Baffles over the Mixture of Turbulent Flows into Stirred Tanks

Laísa Luiz Soares [1], Cesare Biserni [2,*], Roger da Rosa Costa [3], João Américo Aguirre Oliveira Júnior [4], Elizaldo Domingues dos Santos [1] and Marcelo Moraes Galarça [1,3]

[1] Graduate Program in Computational Modeling, Federal University of Rio Grande—FURG, Itália Av., km 8, Rio Grande 96203-900, RS, Brazil; laisaluiz@furg.br (L.L.S.); elizaldosantos@furg.br (E.D.d.S.); marcelo.galarca@riogrande.ifrs.edu.br (M.M.G.)
[2] Department of Industrial Engineering, Alma Mater Studiorum, University of Bologna, Viale Risorgimento 2, 40136 Bologna, Italy
[3] Federal Institute of Education, Science and Technology of Rio Grande do Sul—IFRS, Alfredo Huch Engineer Street, 475, Rio Grande 96201-900, RS, Brazil; roger.costa@aluno.riogrande.ifrs.edu.br
[4] Engineering Simulation and Scientific Software Ltd., Orlando Phillipi St., 100, Florianópolis 88032-700, SC, Brazil; aguirre.eng@gmail.com
* Correspondence: cesare.biserni@unibo.it

Abstract: The present work aims to define strategies for numerical simulation of the mixture of turbulent flows in a stirred tank with a low computational effort, and to investigate the influence of the geometry of four rectangular baffles on the problem of performance. Two computational models based on momentum source and sliding mesh are validated by comparison with experimental results from the literature. For both models, the time-averaged conservation equations of mass, momentum and transport of the mixture are solved using the finite volume method (FVM) (FLUENT® v.14.5). The standard k–ε model is used for closure of turbulence. Concerning the geometrical investigation, constructal design is employed to define the search space, degrees of freedom and performance indicators of the problem. More precisely, seven configurations with different width/length (L/B) ratios for the rectangular baffles are studied and compared with an unbaffled case. The momentum source model leads to valid results and significantly reduces the computational effort in comparison with the sliding mesh model. Concerning the design, the results indicate that the case without baffles creates the highest magnitude of turbulence kinetic energy, but poorly distributes it along the domain. The best configuration, $(L/B)_o$ = 1.0, leads to a mixture performance nearly two times superior than the case without baffles.

Keywords: stirred tank; momentum source model; sliding mesh model; computational modeling; constructal design

Citation: Soares, L.L.; Biserni, C.; da Rosa Costa, R.; Oliveira Júnior, J.A.A.; dos Santos, E.D.; Galarça, M.M. Numerical Study and Geometric Investigation of the Influence of Rectangular Baffles over the Mixture of Turbulent Flows into Stirred Tanks. *Appl. Sci.* **2022**, *12*, 4827. https://doi.org/10.3390/app12104827

Academic Editor: Jianzhong Lin

Received: 21 January 2022
Accepted: 7 May 2022
Published: 10 May 2022

1. Introduction

Tanks with mechanical agitation play an important role, being widely used by chemical, pharmaceutical, food and fuel production industries. The quality of the final product highly depends on the configuration and operating conditions of the tank. The process of improvement involving these tanks requires an accurate understanding of the flow behavior as well as the evolution of the mixture process in space and time [1].

Several geometric configurations for the cross-sectional shape of the tanks have been proposed in the literature, from cylindrical to polygonal. Among the investigated shapes, a cylindrical shape is the most common [2]. Concerning the impellers, different configurations have also been explored, as well as their placement in the tank [3,4].

The flow in these tanks is generally turbulent, and fluid mixing takes place by a combination of mechanisms: convection caused by bulk motion (stirring, for example), molecular diffusion and turbulent diffusion. The processes of chemical reaction, mass transfer, heat transfer, fluid blending, among others, are dramatically affected by the presence of turbulence [5]. Moreover, in these tanks there are specific areas called dead spots where only diffusion takes place. In general, an increase in the momentum of the flow leads to a decrease in dead spots in the volume of the tank, leading to a decrease in mixing time. Therefore, in order to reduce the dead zones and intensify the rate of mixing, baffles are distributed on the tank walls for directing the flow, breaking vortices and contributing to energy dissipation [3,6].

The improvement of stirred tanks aims to decrease the mixing time and energy cost. Fluid mixing is characterized by tracking the dissipation of a passive scalar injected into the volume of the fluid [7]. This approach has been recommended for predicting the mixing time for miscible liquids since it does not require a solution for the phase interface between the fluids [8].

Important studies have been performed to improve the comprehension of the phenomenology of the problem as well as the influence of impellers on power for the tank and mixture of the flow. For instance, ref. [9] presented numerical simulations to investigate transient power consumption characteristics in a stirred tank without baffles. The transient power number was analyzed based on the predicted impeller torque. The results showed that the power number undergoes four stages: plateau value, sharp falling, slow falling and stable stages, which are affected by the velocity of the impeller. Li et al. [10] studied the mixing characteristics in a stirred tank with two six-blade Rushton turbines. The mixing efficiency was predicted using a scalar transport model that accounted for the local and global mixing time in the stirred tank. The flow pattern was affected by changing the tank configurations (e.g., with/without baffles, impeller size and velocity of the impeller), which also had a significant influence on the mixing process and overall mixing time. Javed et al. [11] numerically studied turbulent mixing of a passive scalar in a stirred tank by a six-blade Rushton turbine. The mixture simulation was performed by injecting an inert tracer at a location on the upper surface of the tank. The predicted evolution of the tracer concentration over time and mixing times were analyzed at various points inside the tank. The results showed that the concentration of the tracer exhibited initial fluctuations that decreased with time and eventually reached a steady state value that represented the concentration of the fully mixed tracer. Considering that mixing time is defined as the time required for the concentration variance to reach a predetermined value, the results indicated that full mixing was achieved between 3.1 s and 4.8 s. Furthermore, some advances have also been made towards the most representative phenomenological conditions for turbulent flow. For example, ref. [12] numerically evaluated the mixing characteristics and the mixing time for a tank with a Rushton turbine using large eddy simulation (LES) to approach turbulent flow. Recently, ref. [13] developed a computational fluid dynamics (CFD) code with a Euler–Euler model to tackle two-phase flow and mixing of liquid and bubbles in a stirred tank reactor. A sliding mesh approach was also used to simulate the effect of the impeller on fluid flow. The authors concluded that the fluid dynamic behavior and the mixing of both phases around the two blades and in the main tube of the reactor were physically plausible.

The influence of the geometric configuration of the impellers has also been investigated. In this realm, ref. [14] evaluated the position of the impeller from the bottom of the tank and disc thickness, as well as the influence of the Reynolds number on the flow field and energy consumption using a Rushton turbine. Gu et al. [15] presented a numerical simulation of the mixing process in a stirred tank and considered the effects of impeller speed, type, spacing, blade tilt angle and blade shape. The authors found an impeller spacing and impeller blade tilt angle most appropriate for the solid-liquid suspension process. Subsequently, ref. [16] performed a numerical study of the influence of an impeller with a regular blade and another with fractal blades on power

consumption, and showed that fractal blades reduced torque compared to regular blades, since the drag coefficient of the fractal blade was distinctly lower than a regular blade. Till et al. [3] studied the effect of the number of blades for the impeller and different rotation speeds on the mixing efficiency and power consumption in a stirred tank. They concluded that the electrical power requirement for an impeller depended largely on the shape and the size of the impeller and, of course, the rotational speed. Moreover, an increase in mixing led to an exponential increase in the required power. Recently, ref. [17] studied the effect of different kinds of agitators on turbulent flow in stirred tanks, with and without baffles. The hydrodynamics behavior was induced by four different kinds of agitator: a Rushton turbine (RT), a circular blade turbine (CBT), a diverging triangular blade turbine (DTBT) and a converging triangular blade turbine (CTBT).

In spite of the importance of baffles for the mixing of fluids in tanks, this kind of analysis is still very sparse in the literature. For instance, ref. [18] numerically studied two agitated tanks with and without baffles, varying the Reynolds number between laminar and turbulent flow in order to study the influence of these baffles on the power and pumping numbers. The authors concluded that, until a certain Reynolds number was achieved, the presence or not of baffles did not have a significant influence on the power. The magnitude of the power and pumping numbers started to differ in the presence of baffles when the flow was in transition, and drastically different values occurred in a totally turbulent flow. Subsequently, ref. [2] studied the influence of the stirred tank shape (cylindrical and polygonal) with and without baffles (vertical and circular baffles). A circular baffle has a format similar to a ring placed around the impeller and at a certain distance from the bottom of the tank. This ring was cut at different angles (20°, 30° and 45°), thus obtaining different size of baffles for each cutting angle. The authors concluded that the polygonal shape produced results similar to those of the cylindrical tank. In addition, the results showed that power consumption and vortex size decreased when the circular baffle was cut at an angle of 20°. For the rectangular baffles, the power consumption was lower for tanks with only one baffle than two, three or four baffles.

Despite the above mentioned investigations, few studies have investigated the effect of the geometrical configuration of the baffles on the mixing process and turbulent flow in stirred tanks, and even fewer have considered the application of constructal design [19,20]. Constructal design is a method used to apply the physical principle of design to any finite-sized flow system. Constructal law states that for a finite-sized flow system to persist, i.e., to live, its design must evolve in such a way as to easily access the internal currents of the thermodynamic flow system [19,21]. This unifying principle of design has been applied to predict designs in nature (trees, branches, vascular tissues and animal design), social organization (flow of goods, people and information and organizational structures) and engineering problems (renewable energy, fluid mechanics and heat transfer, heat exchangers, marine and aerodynamical structures and manufacturing processes) [22,23].

Considering the wide applicability of constructal design, it is expected that this method can guide the theoretical recommendations for the influence of the design of rectangular baffles inserted in stirred tanks on mixture performance. More precisely, the present study has two main purposes. The first is the investigation of strategies for numerical simulation of mixing in turbulent flows in stirred tanks that reproduces adequately the fluid dynamic behavior of turbulent flow with the lowest computational effort. The second is to understand the influence of geometrical configurations on the mixing of turbulent fluid flow along the domain by means of constructal design, seeking to maximize mixing. The constructal design method is based on a physical universal principle (constructal law of design and evolution) for the generation of design in any finite-sized flow system [18–22]. This method is used to obtain new recommendations on the influence of design of rectangular baffles on the mixture of turbulent flows in a tank. To the best of the authors' knowledge, this kind of investigation has not been previously performed in the literature. Therefore, the main contributions here are the definition of

strategies to speed up the results for fluid dynamic behavior, including the prediction of performance indicators for the mixture, and to obtain new recommendations for the design of rectangular baffles to improve the mixture of turbulent flows in stirred tanks.

To investigate the mixing inside an agitated tank, a species transport model is used in which a passive scalar is injected when the flow reaches the steady state, and its distribution is monitored over time. The idea is to conduct the mixture until it equalizes the concentration differences between the passive scalar and the fluid in neighboring regions of the mixture. This concentration is calculated from the standard deviation of the mass fraction of the tracer in the tank volume. The time-averaged conservation equations of mass and momentum are solved with the finite volume method (FVM); more precisely with the commercial package FLUENT v.14.5 [24,25]. The isothermal flow is considered three-dimensional, turbulent and incompressible. For closure of turbulence, the RANS (Reynolds-averaged Navier–Stokes) standard k–ε model was employed. A momentum source model applying a UDF (user defined function) was also implemented in this work to simulate the influence of the impeller on the fluid in the tank. This model was compared to a sliding mesh model, also developed in this work, and both were verified and validated with numerical and experimental data from the literature.

2. Problem Description and Mathematical Modeling

The stirred tank used in this work is a standard cylindrical configuration with dimensions given by Figure 1 and Table 1. Figure 1a shows the upper view of the tank, and Figure 1b is a cut view of section A–A. The height of the tank is equal to its diameter, $H = 2R$. The working fluid is water at atmospheric pressure with thermophysical properties at a temperature of $T = 293$ K. The impeller is a six-bladed Rushton turbine with standard dimensions (often found in the literature) mounted at a certain height from the tank bottom (C). If geometric similarity is kept, the flow system can be fully described by the Reynolds flow number $Re_D = \rho N D^2/\mu$. For this work, the impeller speed is $N = 300$ rpm (5 rps), which is imposed in an anticlockwise direction, ρ is the water density, μ is the dynamic viscosity and D is the impeller diameter. The simulations were performed here with a Reynolds number of $Re_D = 47{,}790$.

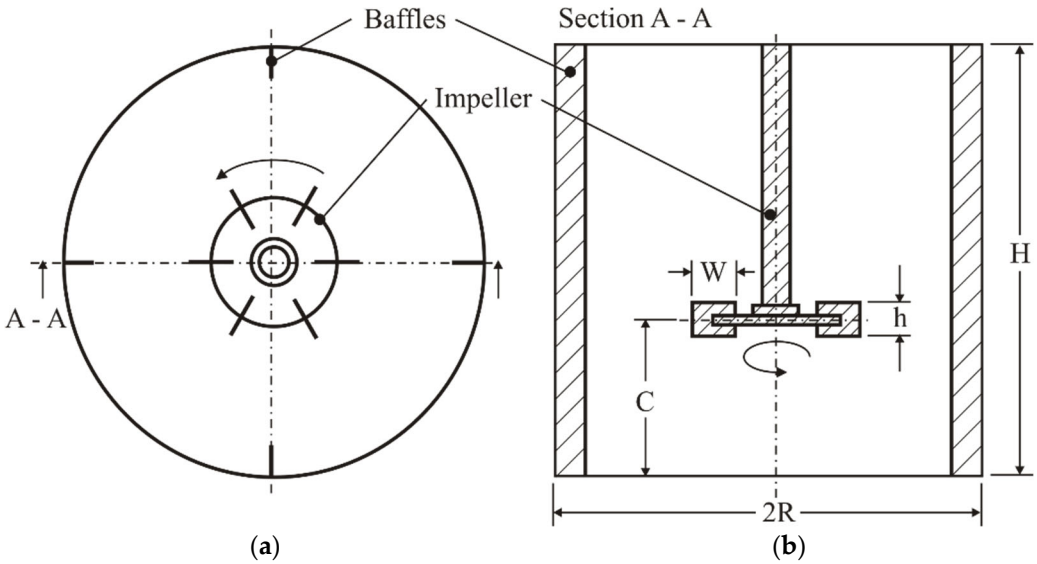

Figure 1. Dimensions of the stirred tank with four baffles: (**a**) upper view (**b**) view of Section A–A.

Table 1. Dimensions (m) of the tank shown in the Figure 1.

2*R*	*H*	*D*	*C*	*W*	*B*	*H*
0.296	0.296	2*R*/3	2*R*/3	*D*/4	2*R*/10	*D*/5

The side, top and bottom walls of the tank, as well as the surfaces of the baffles, have no-slip and impermeability boundary conditions. For all cases, the flow is at rest for the initial condition.

The turbulent, incompressible, isothermal flows in the three-dimensional domain of the tank are modeled by the time-averaged conservation equations of mass and momentum, as defined by [26]:

$$\frac{\partial \bar{u}}{\partial x} + \frac{\partial \bar{v}}{\partial y} + \frac{\partial \bar{w}}{\partial z} = 0 \tag{1}$$

$$\frac{\partial \bar{u}}{\partial t} + u\frac{\partial \bar{u}}{\partial x} + v\frac{\partial \bar{u}}{\partial y} + w\frac{\partial \bar{u}}{\partial z} = -\frac{1}{\rho}\frac{\partial \bar{p}}{\partial x} + (\vartheta + \vartheta_T)\left(\frac{\partial^2 \bar{u}}{\partial x^2} + \frac{\partial^2 \bar{u}}{\partial y^2} + \frac{\partial^2 \bar{u}}{\partial z^2}\right) + f \tag{2}$$

$$\frac{\partial \bar{v}}{\partial t} + u\frac{\partial \bar{v}}{\partial x} + v\frac{\partial \bar{v}}{\partial y} + w\frac{\partial \bar{v}}{\partial z} = -\frac{1}{\rho}\frac{\partial \bar{p}}{\partial x} + (\vartheta + \vartheta_T)\left(\frac{\partial^2 \bar{v}}{\partial x^2} + \frac{\partial^2 \bar{v}}{\partial y^2} + \frac{\partial^2 \bar{v}}{\partial z^2}\right) + f \tag{3}$$

$$\frac{\partial \bar{w}}{\partial t} + u\frac{\partial \bar{w}}{\partial x} + v\frac{\partial \bar{w}}{\partial y} + w\frac{\partial \bar{w}}{\partial z} = -\frac{1}{\rho}\frac{\partial \bar{p}}{\partial x} + (\vartheta + \vartheta_T)\left(\frac{\partial^2 \bar{w}}{\partial x^2} + \frac{\partial^2 \bar{w}}{\partial y^2} + \frac{\partial^2 \bar{w}}{\partial z^2}\right) + f \tag{4}$$

where $\bar{u}$, $\bar{v}$ and $\bar{z}$ are the time-averaged velocities in x, y and z directions, p is the pressure, ϑ is the kinematic viscosity, f is a source term of momentum and ϑ_T is the turbulent viscosity of the fluid flow, which is given by:

$$\vartheta_T = C_\mu \frac{k^2}{\varepsilon} \tag{5}$$

where C_μ is an ad hoc constant, k is the turbulent kinetic energy and ε is the turbulent kinetic energy dissipation rate. For closure of turbulence, a standard k–ε model was used that determines the k and ε by the solution of two transport equations [27,28]:

$$\frac{\partial(\rho k)}{\partial t} + \nabla(\rho \vec{v} k) = \nabla\left(\frac{\mu_T}{\sigma_k}\nabla k\right) + G_k - \rho\varepsilon + S_k \tag{6}$$

$$\frac{\partial(\rho \varepsilon)}{\partial t} + \nabla(\rho \vec{v} \varepsilon) = \nabla\left(\frac{\mu_T}{\sigma_\varepsilon}\nabla \varepsilon\right) + \frac{\varepsilon}{k}(C_{1\varepsilon}G_k - C_{2\varepsilon}\rho\varepsilon) + S_\varepsilon \tag{7}$$

where G_k represents the generation of turbulence kinetic energy due to the mean velocity gradients, $G_{1\varepsilon}$ and $G_{2\varepsilon}$ are constants, σ_k and σ_ε are the turbulent Prandtl numbers for k and ε, respectively, and S_k and S_ε are source terms.

3. Modeling of Momentum Source Model

For the momentum source model, an equation is compiled into a user defined function (UDF). The subroutine of UDF is basically written in C programming language, which can be dynamically loaded with the solver in order to improve the standard features of the software [24]. In this way, it is possible to define a source term that describes the rotation of the impeller inside the tank without the need to use a sliding mesh. The equations for the model are defined by [29]:

$$dF = \rho \cdot dS \cdot u(u - v_\theta) \tag{8}$$

where dF is the force exerted by the impeller, dS is the area element on the blade surface and v_θ is the tangential velocity.

To account for the drag effect on fluid flow, a friction resistance equation is introduced to calculate the friction force as follows:

$$df = \frac{1}{2}\rho \cdot v_r^2 \cdot C_f \cdot dS \tag{9}$$

where v_r is the radial velocity and C_f is local resistance coefficient related to Re_x, which is calculated by:

$$C_f = 0.664 \cdot Re_x^{-0.5} \cdot Re_x \leq 5 \times 10^5 \quad (10)$$

$$C_f = 0.0557 \cdot Re_x^{-0.2} \cdot 5 \times 10^5 < Re_x < 1 \times 10^7 \quad (11)$$

where $Re_x = \rho v_x x/\mu$, x is the distance between cell center and the center of rotation axis.

3.1. Species Transport Model

For the numerical analysis of flow homogenization, a species transport model (without chemical reactions) implemented in the FLUENT® software was used. In this model, it is possible to predict the local mass fraction of the species that is being transported through the solution of a convection-diffusion equation given by [24]:

$$\frac{\partial \rho Y_i}{\partial t} + (\nabla \rho \vec{v} Y_i) = -\nabla \vec{J_i} \quad (12)$$

where Y_i is the local mass fraction of species i and $\vec{J_i}$ is the diffusion flux of species i. For turbulent flow, $\vec{J_i}$ is given by:

$$\vec{J_i} = -\left(\rho D_{i,m} + \frac{\mu_T}{Sc_t}\right) \nabla Y_i \quad (13)$$

where $D_{i,m}$ is the mass diffusion coefficient for species i in the mixture and Sc_t is the turbulent Schmidt number.

3.2. Constructal Design Application to the Problem

As previously mentioned, constructal design is the method used to apply the constructal law of design and evolution [19,20]. The method consists of the investigation of geometry subjected to constraints (global and local), which define the limitations and search space for the variation in geometry given by the degrees of freedom, and the performance indicators, which are used to define the maximization of the internal currents of the flow system.

The main steps for the geometric investigation performed here are illustrated in the flowchart in Figure 2. Steps 1 to 3 consists of the definition of the flow system and performance indicators, and steps 4 and 5 define the constraints of the problem, degrees of freedom and the main parameters of the physical problem. At the same time, it is necessary to understand the physical problem and define a method for its solution (numerical in the present work). After the fifth step, it is important to define whether the problem is optimized or not, as well as the number of cases required to investigate the influence of degrees of freedom, constraints and parameters on the performance indicators. It is worth mentioning that constructal design is not an optimization method, but a method for geometrical investigation based on the principle of constraints and objectives [30,31]. Here, the method is applied to the geometric investigation of only one degree of freedom (L/B) on the performance of turbulent flow in stirred tanks due to the high computational effort required for each simulated case. The last three steps (6 to 8) consist of defining the number of cases to be studied, performing the numerical simulations for each configuration and investigating the effect of the degrees of freedom on the performance indicators.

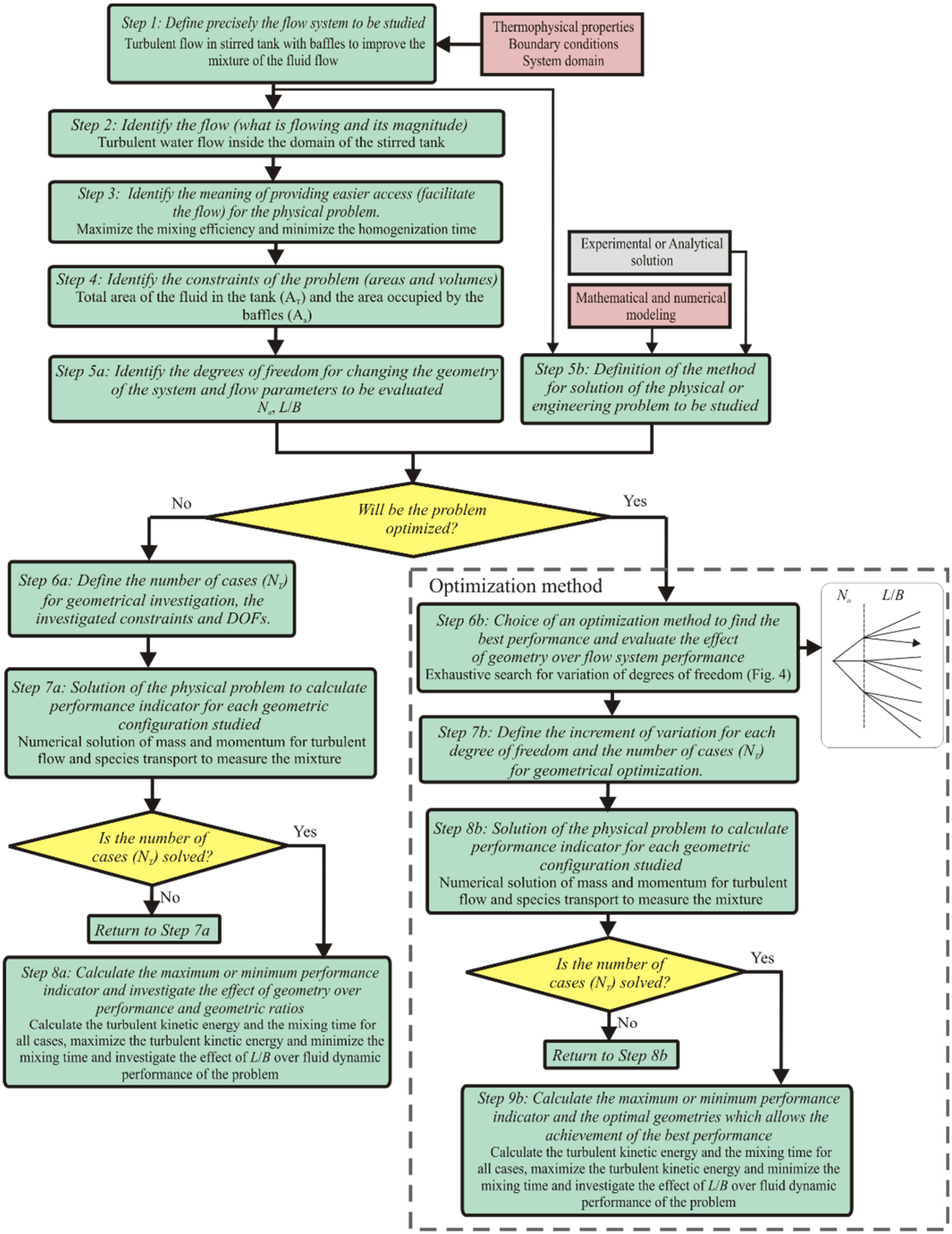

Figure 2. Flowchart illustrating the application of the constructal design for geometrical investigation of the present problem.

It is considered here that the problem is subject to two area constraints: the total area in the tank where the baffle can be placed (A_T) and the area occupied by the baffles (A_a). A sketch of the cross-sectional area of the tank and the above-mentioned areas is illustrated in Figure 3. The constraint areas are given by Equations (14) and (15) as follows:

$$A_T = A_F - A_I \tag{14}$$

where A_F is the total fluid area of the tank and A_I is the area that can be occupied by the impeller.

$$A_a = N_a \cdot L \cdot B \tag{15}$$

where N_a is the amount of baffles, L is the baffle width and B is the baffle length.

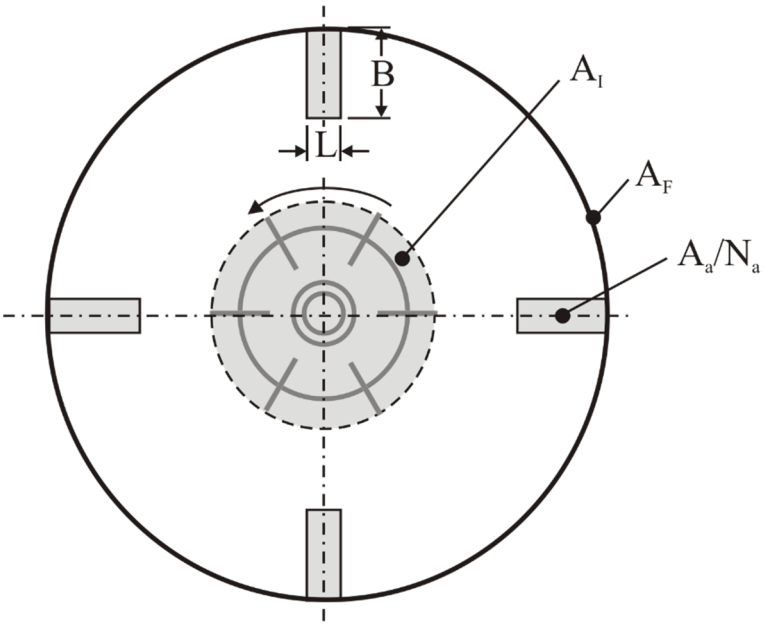

Figure 3. Schematic representation of the computational domain with four baffles used in the definition of the geometrical investigation.

The dimensions L and B are defined considering the constraints of the area occupied by the baffles. Thus, there is an equation and three variables, and it is necessary to define two degrees of freedom to solve this problem (N_a and L/B) as defined by the following equations:

$$B = \left(\frac{A_T \cdot \emptyset}{N_a \cdot \left(\frac{L}{B}\right)} \right)^{1/2} \tag{16}$$

$$L = \left(\frac{L}{B}\right) \cdot B \tag{17}$$

where $\emptyset$ is the ratio between the areas occupied by the baffles and the total area where the baffles can be placed, which is given by the following equation:

$$\emptyset = \frac{A_a}{A_T} \tag{18}$$

In addition, the dimensions L and B have a limit to vary, i.e., B can be varied so that its maximum length does not exceed the area occupied by the impeller. The limit of L is the maximum width before exceeding the tank wall limits.

Thus, with the degrees of freedom defined, the geometric evaluation takes place by varying one of them (L/B) and keeping the other fixed (N_a). The constraints of the area are

also fixed. Here, the investigation is limited to $N_a = 4$ for the effect of L/B on the standard deviation of the mixture inside of the tank domain and the homogenization time, which can be minimized. Figure 4a shows the tree of simulations performed from the application of constructal design, Figure 4b illustrates the dimensions of the baffles inserted in the tank, and Table 2 shows the dimensions of baffles used in each case. It is worth mentioning that the superior limit for the ratio L/B is restricted to $L/B = 1.0$ to avoid the construction of a large part of the baffle out of the stirred tank and violation of the baffle area (A_a) constraint.

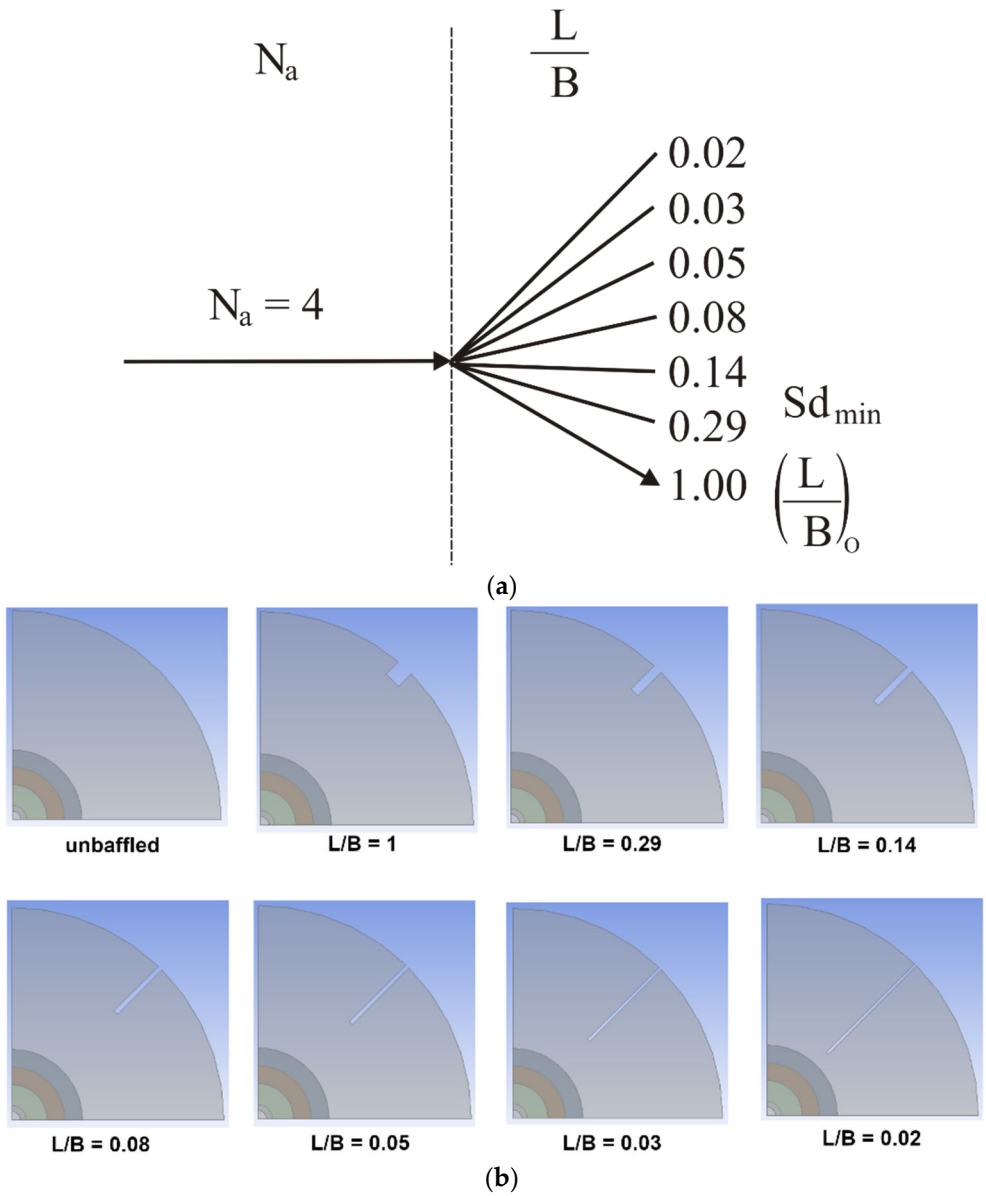

Figure 4. Scheme for the different configurations studied: (**a**) flowchart of configurations defined with constructal design; (**b**) illustration of the cross sectional area of the tank for the different investigated cases.

Table 2. Baffles dimensions (m) from the application of the Constructal Design method.

	Case 1 *L/B* = 1	**Case 2** *L/B* = 0.29	**Case 3** *L/B* = 0.14	**Case 4** *L/B* = 0.08	**Case 5** *L/B* = 0.05	**Case 6** *L/B* = 0.03	**Case 7** *L/B* = 0.02
L	0.01237	0.00666	0.00463	0.00350	0.00276	0.00214	0.00175
B	0.01237	0.02297	0.03306	0.04374	0.05533	0.07143	0.08749

4. Numerical Modeling

In this work, two numerical models are used to simulate the mixing tank operation: sliding mesh and momentum source term. For the momentum source model, the fluid motion is caused by the imposition of a momentum source, which mimics the impeller in the region occupied by the blades. For the model with sliding mesh, a constant angular velocity is imposed on the region that contains the impeller.

The treatment of the advective terms considers a second order upwind, whereas an implicit formulation of the first order is applied to the transient terms. The coupling pressure-velocity SIMPLE is used. A numerical solution convergence is reached when the residuals achieve the values of 1.0×10^{-4} for continuity, and 1.0×10^{-5} for momentum and turbulence for every time-step. The time step is $\Delta t = 1.0 \times 10^{-2}$ s, which was recommended by previous studies in the literature for similar fluid dynamic conditions [3,10,11,14].

Both numerical models were simulated by a computer with an architecture of x86_64, Intel Core i7-5930k, CPU 3.50 GHz with 12 CPUs. Thus, the computational time required to simulate 3.5 s was 240 h for the sliding mesh model and 5 h for the momentum source model. Therefore, the momentum source model requires about 2% of the computational effort required by the sliding mesh model. This is a great advantage, mainly for the geometric investigation purposes. Therefore, if the computational model produces results in agreement with the literature, it can be used to provide new design recommendations for the mixture processes in stirred tanks.

4.1. Sliding Mesh Model

In the sliding mesh model, shown in Figure 5, the computational domain of the tank is divided into two regions that are treated separately: the region of the impeller, and the region of the tank which includes flow, the surrounding walls and the baffles. The mesh region, which contains the impeller, rotates with constant velocity while the other region (computational domain) is fixed. This method, in general, is able to predict flow evolution over time, but it has a high computational cost. The mesh with an independent solution for this model (following recommendations from the literature [11,29]) has 586,483 cells, which can be seen in Figure 6.

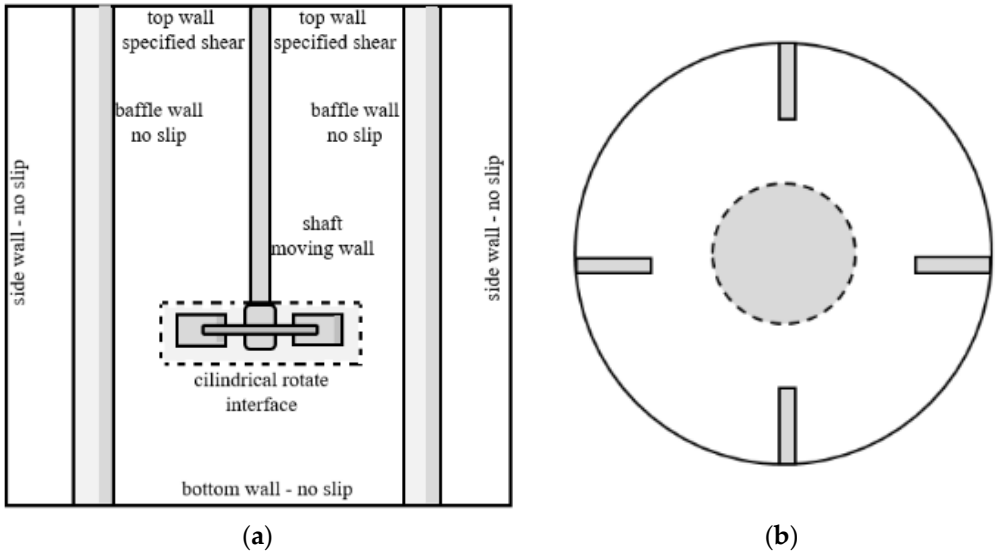

Figure 5. Computational domain scheme of the sliding mesh model. (**a**) Side view of the tank. (**b**) Top view of the tank.

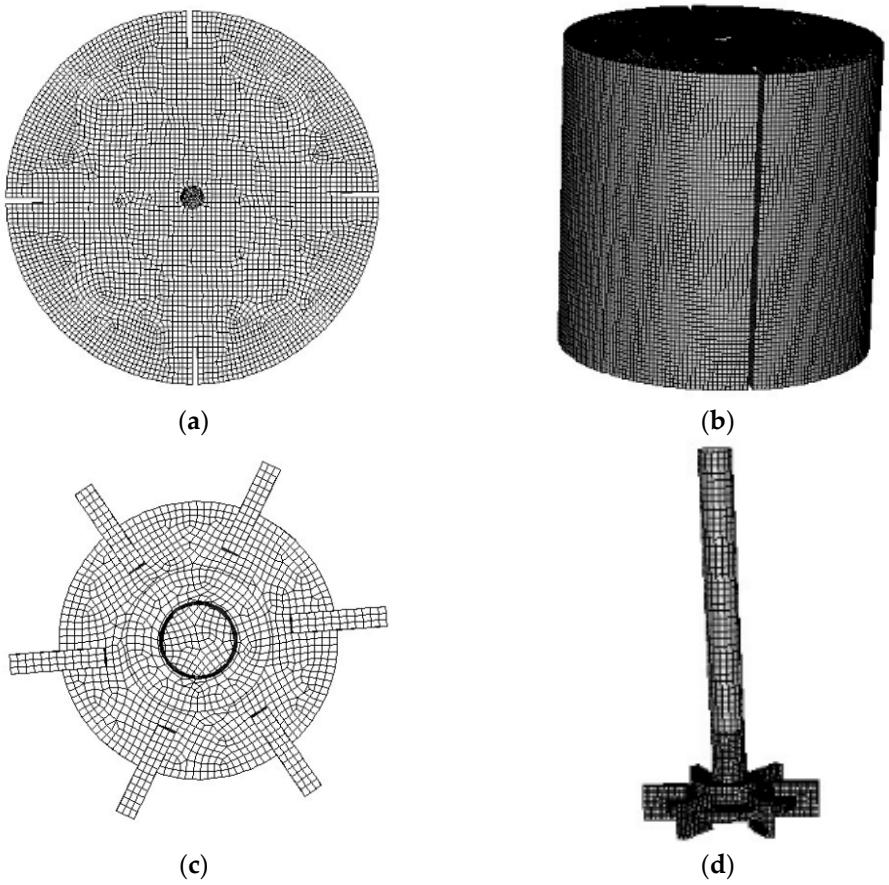

Figure 6. Mesh for the sliding mesh model. (**a**) Top view of the tank. (**b**) Side view of the tank. (**c**) Top view of the impeller. (**d**) Side view of the impeller.

4.2. Momentum Source Model

For the momentum source model, illustrated in Figure 7, the impeller is replaced by a disc. In the disc region, a source term, represented by Equations (8)–(11), is imposed on the momentum equation to mimic impeller rotation. Since the mesh is completely fixed in this model, i.e., without regions with imposed rotation, the computational cost is significantly lower than that required for a rotation region. It is also possible to further reduce the computational cost by considering it as a symmetry condition problem so that it can be simulated with just a quarter of the computational domain.

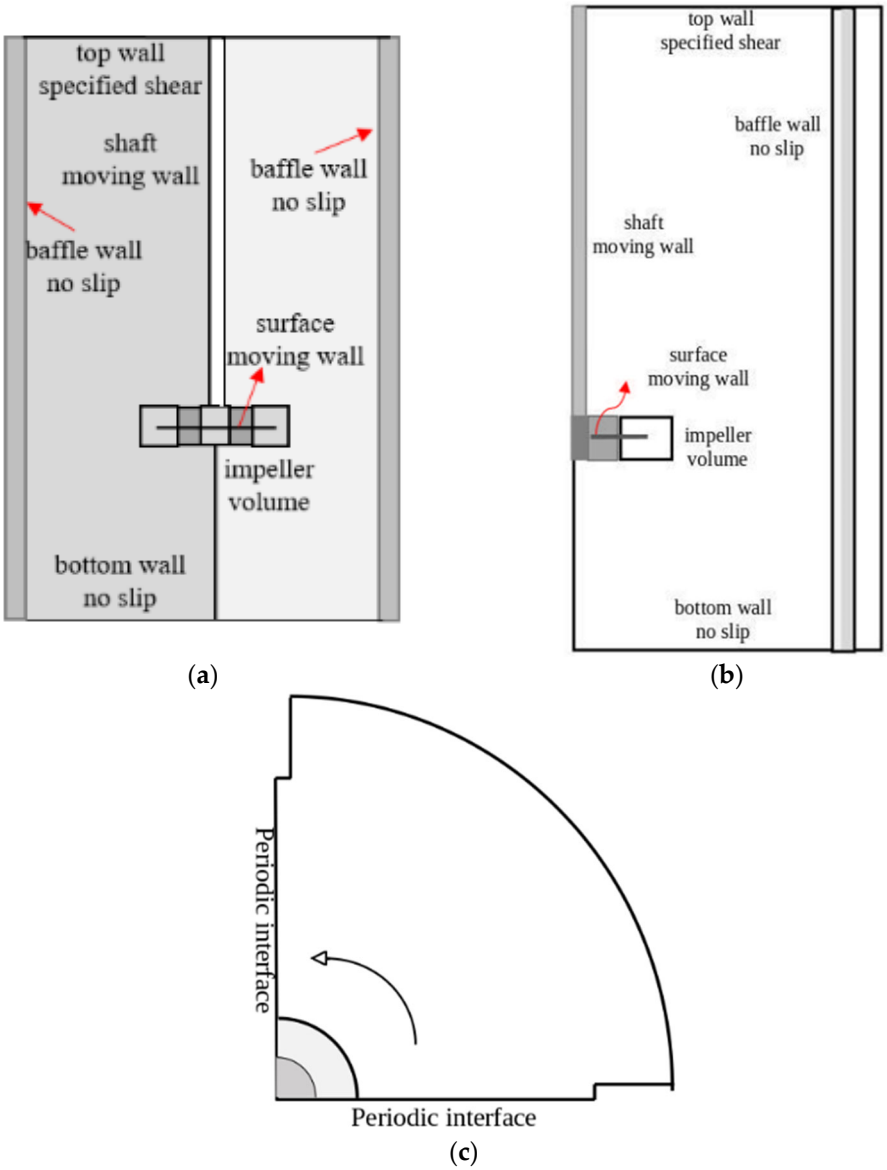

Figure 7. Computational domain scheme for the momentum source model. (**a**) View of the two cut interfaces 90°, (**b**) side interface cut 90° and (**c**) top view.

Grid Independence Study

One of the most important steps in numerical simulation is the achievement of an independent mesh. The great challenge is to find a mesh sufficiently refined so that the results generated are in good agreement with experimental or other numerical results without a high computational cost. In general, there is a moment where the numerical results are practically unchanged when compared to a previous mesh (that was coarser). Thus, the coarser mesh solves the problem with a relatively low error and with much less computational effort [32]. It is worth mentioning that, for both models, the near wall region is modeled considering a scalable wall function and the maximum wall plus is $y^+ \leq 30.0$.

Recently, a statistical method was defined for quantifying the influence of grid discretization on numerical problems that has been considered highly effective for quantifying how close any solution for the investigated mesh is to the independent region [32,33]. This technique is named the grid convergence index (GCI) and it has been successfully used in recent studies to predict suitable meshes for numerical studies [34]. A total of five

steps are required to apply this method, and all calculation criteria are defined by the norm ASME V&V [32]:

Step 1: Define a representative cell, mesh or grid size, h.

Step 2: Select three significantly different sets of grid resolutions and run simulations to determine the values of key variables important (φ) to the objective of the simulation study. It is desirable that the grid refinement factor ($r = h_{coarse}/h_{fine}$) should be greater than 1.3.

Step 3: Let $h_1 < h_2 < h_3$ and $r_{21} = h_2/h_1$, $r_{32} = h_3/h_2$ and calculate the apparent order, p, of the method by:

$$p = \left[\frac{1}{\ln(r_{21})}\right][\ln|\gamma_{32} - \gamma_{21}| + q(p)] \tag{19}$$

$$q(p) = \ln\left(\frac{r_{21}^p - S}{r_{32}^p - S}\right) \tag{20}$$

$$S = 1 \cdot \text{sign}(\gamma_{32}/\gamma_{21}) \tag{21}$$

where sign is a function that returns 1 if the value is positive, −1 if the value is negative or 0 if a value is 0, $\gamma_{32} = \varphi_3 - \varphi_2$, $\gamma_{21} = \varphi_2 - \varphi_1$ and φ_k denotes the simulation value of the variable on the *k*th grid. Note that $q(p) = 0$ for $r = constant$. This set of three equations can be solved using fixed point iteration with the initial guess equal to the first term (i.e., $q = 0$).

A minimum of four grids are required to demonstrate that the observed order p is constant for a simulation series.

Step 4: Calculate the extrapolated values from the equation:

$$\varphi_{ext}^{21} = (r_{21}^p \varphi_1 - \varphi_2)/(r_{21}^p - 1) \tag{22}$$

Step 5: Calculate and report the following error estimates along with the observed order of the method p. Approximate relative error may be cast as a dimensionless form or in dimensioned form respectively given by:

$$e_a^{21} = \left|\frac{\varphi_1 - \varphi_2}{\varphi_1}\right| \tag{23}$$

$$e_a^{21} = |\varphi_1 - \varphi_2| \tag{24}$$

The fine grid convergence index is calculated as follows:

$$GCI_{fine}^{21} = \frac{Fs \cdot e_a^{21}}{r_{21}^p - 1} \tag{25}$$

where $Fs = 1.25$ is the factor of safety.

For the present study, the application of the GCI method is presented in Table 3. The magnitude of GCI between meshes 1 and 2 was below 1.0% and the asymptotic range of convergence was around 1.0, which, according to literature [32,33], indicates the mesh is in the independent region.

Table 3. Results of the application of the GCI method.

Mesh 1	Mesh 2	Mesh 3	r_{32}	r_{21}	p	GCI %
5,484,258 cells	1,878,417 cells	610,767 cells	1.45	1.42	2.82	0.1027

In order to investigate the influence of the grid on the local conditions of fluid flow, Figure 8a,b show the mean radial and tangential velocity profiles, respectively, obtained in the impeller region (z = 0.08 m) with the three different grids employed here, i.e., the velocity in two different directions of the domain for a specific placement of the domain. The results are calculated when the fluid flow reaches the steady state. Then, the last time

interval of t = 1.5 s is used to obtain the mean velocity profiles. The solution takes into account initiation values of 0.01 m²/s² and 0.001 m²/s³ for turbulence kinetic energy and dissipation rate, respectively. Moreover, Figure 9 shows the fields of turbulent kinetic energy in a vertical plane (r–z) for the baffle region predicted with the three investigated meshes comprising 610,767 cells (Figure 9a), 1,878,417 cells (Figure 9b) and 5,484,258 cells (Figure 9c). The results in Figures 8 and 9 show that there are no significant local differences when Mesh 1 and Mesh 2 are compared. However, some localized differences in the velocity profiles, mainly for the tangential one, and for the fields of turbulent kinetic energy were noticed for the coarser mesh. As a consequence, the mesh with 1,878,417 elements was chosen since it had fewer deviations than the coarse mesh (Mesh 3) and required a lower computational effort than Mesh 1. The independent mesh used here can be seen in the Figure 10.

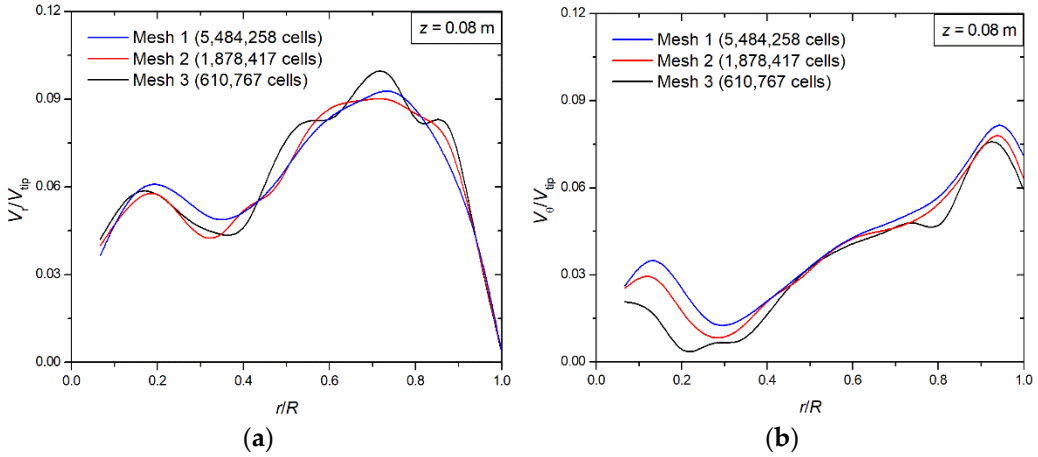

Figure 8. Results of mean velocity profiles obtained with the present code at z = 0.08 m for three different grids: (**a**) radial velocity, (**b**) tangential velocity.

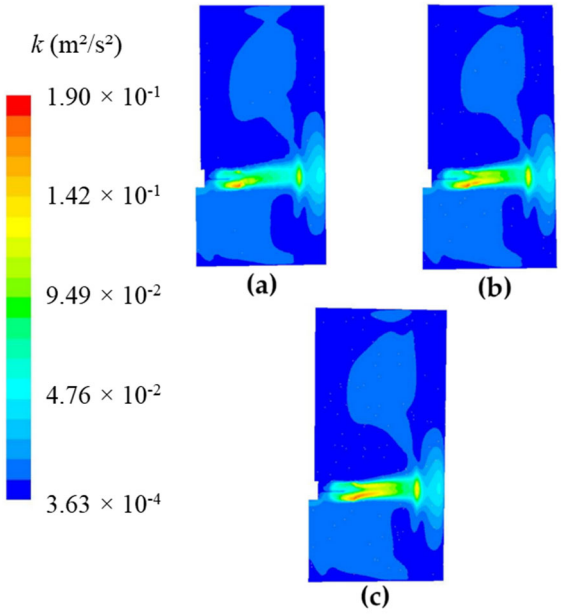

Figure 9. Turbulent kinetic energy fields obtained for three different mesh refinements: (**a**) 610,767 cells, (**b**) 1,878,417 cells, (**c**) 5,484,258 cells.

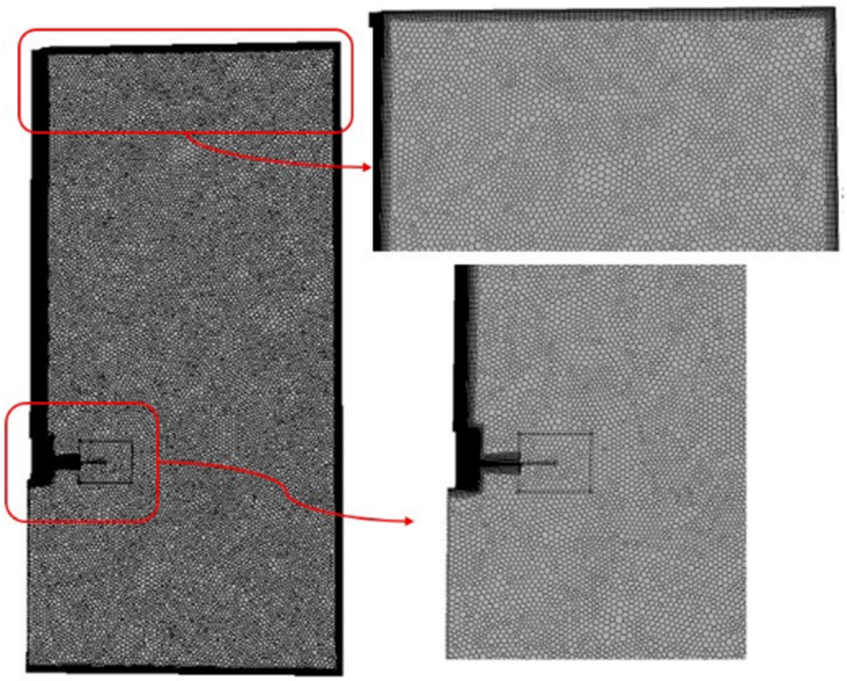

(**a**)

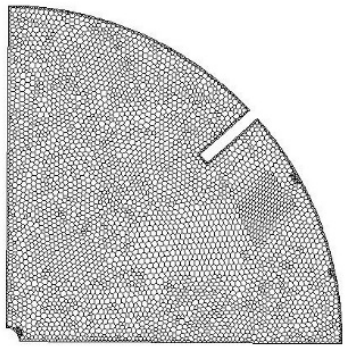

(**b**)

Figure 10. Independent mesh chosen from the GCI method. (**a**) Side view of the tank. (**b**) Top view of the tank.

4.3. Species Transport Model

The species transport model, included in the FLUENT® software package, allows the user to predict the distribution of a local mass fraction, for one or more species, with or without chemical reactions, to be added to the system [24]. Therefore, a tracer was added in the flow without affecting its fluid dynamic behavior. On the other hand, the tracer is affected by the flow and spread in the tank. Thus, the analysis of the species dispersion is given by the mass fraction variance.

5. Results and Discussion

5.1. Development and Validation of the Numerical Models

In the first step, validation was performed with both models. However, for geometrical investigation cases, the momentum source model was solely used. The main difference between the two models lies with the fact that simulations with sliding mesh require a longer processing time than the imposed momentum source model. One reason for this difference is related to the moving interface between the sliding and fixed region. Moreover, it is necessary to simulate the whole computational domain. In contrast, the momentum source model allows the mesh to be well refined since the domain can be simulated by one quarter of the tank and the geometry is simpler than the sliding mesh model.

The velocity fields obtained were compared with the numerical and experimental solutions presented by [10]. For this comparison, the velocity was normalized with $V_{tip} = \pi DN = 1.54$ m/s.

In Figures 11–14, the time-averaged profiles for radial, tangential and axial velocities, and turbulence kinetic energy, respectively, are shown as a function of the radial coordinate for different heights of the tank. In general, the results obtained with the developed models presented similar behavior with the experimental and numerical results predicted by Javed et al. [11].

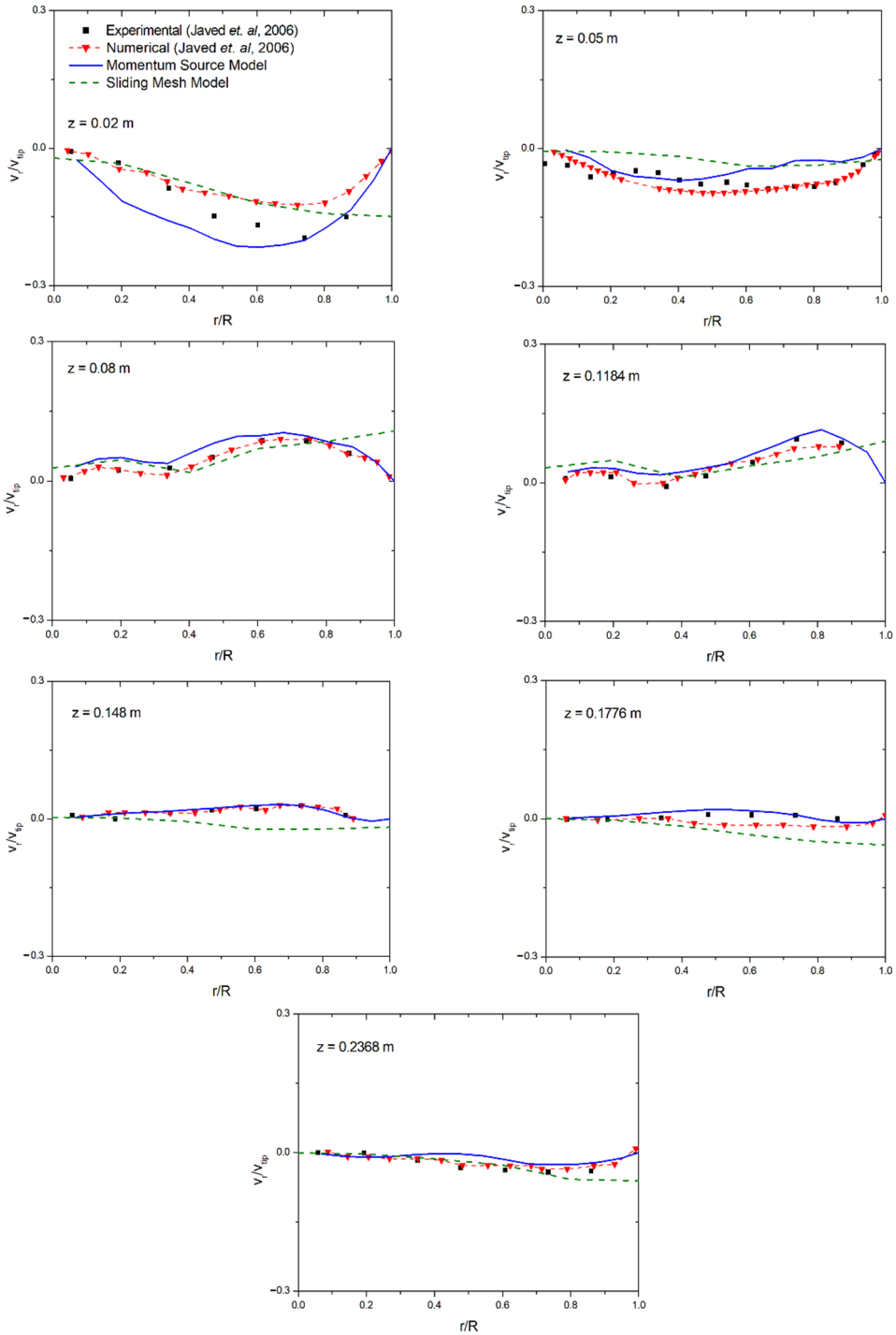

Figure 11. Results for radial velocity profiles obtained with the present code and those predicted by Javed et al. [11].

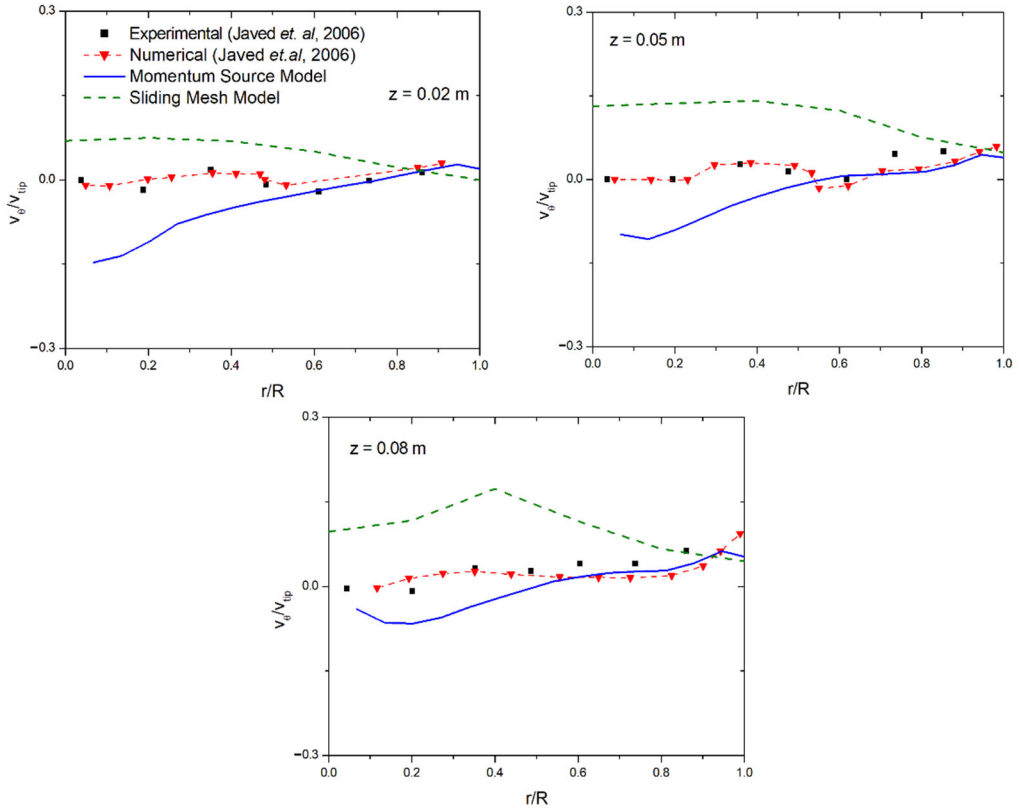

Figure 12. Results for tangential velocity profiles obtained with the present code and those predicted by Javed et al. [11].

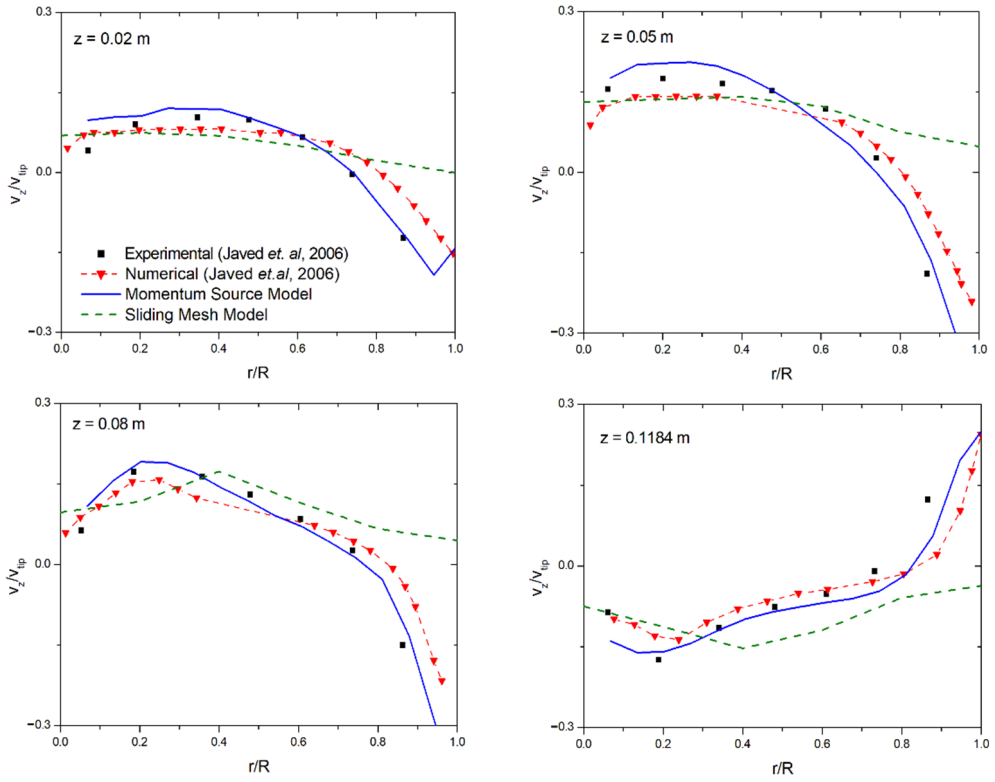

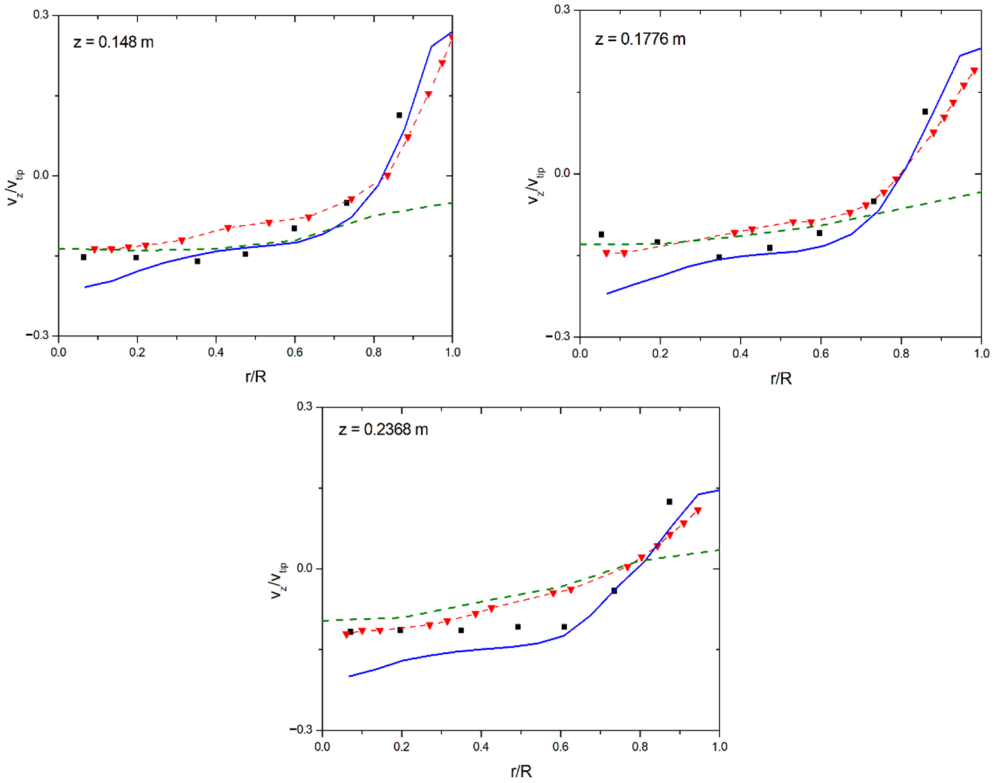

Figure 13. Results for axial velocity profiles obtained with the present code and those predicted by Javed et al. [11].

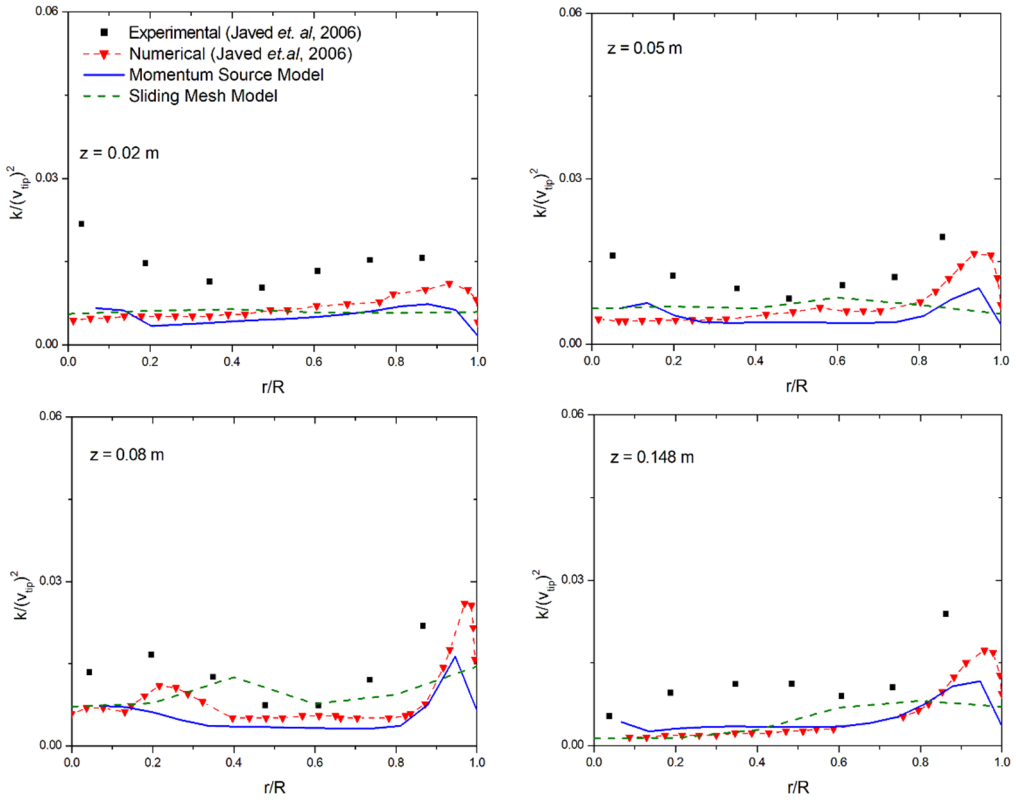

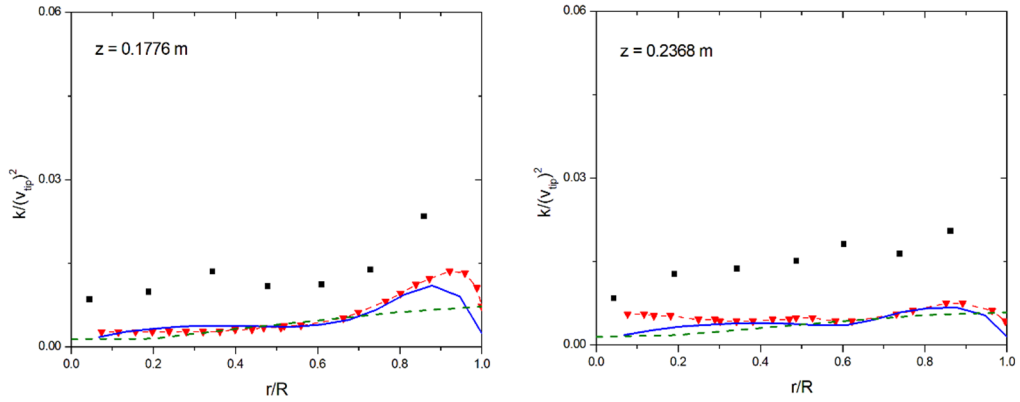

Figure 14. Results for turbulence kinetic energy profiles obtained with the present code and those predicted by Javed et al. [11].

There is a difference in agreement between the sliding mesh model and the momentum source model compared to the data presented in the literature. The momentum source model was able to more efficiently predict velocity and turbulence kinetic energy profiles. One possible reason for the deviations found for the sliding mesh model concerns the difficulty of generating refined meshes, which is more complicated for the sliding mesh since the entire domain is simulated and the physical surfaces of the impeller must be built in the domain. In this sense, the computational cost for a more refined mesh in sliding model would be much higher, which would become prohibitive for future geometrical investigation. The results also demonstrate that the momentum source model presented a good agreement with the numerical and experimental solutions reported in the literature. Therefore, the model is considered valid.

Once the momentum source model was able to reproduce with some efficiency the flow in the tank at a much lower computational cost, it was used to test different geometrical configurations in the present work.

Figure 15a shows the velocity magnitude field in the vertical plane (between the baffles), and Figure 15b depicts the horizontal plane (at impeller height). The flow behavior shown in Figure 15a is similar to the literature [29], showing the formation of two vortices when the fluid reaches the region of the tank wall. Part of the fluid goes to the top of the tank, forming a vortex above the impeller, and the other part of the fluid goes to the bottom of the tank, forming another vortex below the impeller. Afterwards, the fluid tends to return to the impeller region to repeat this behavior.

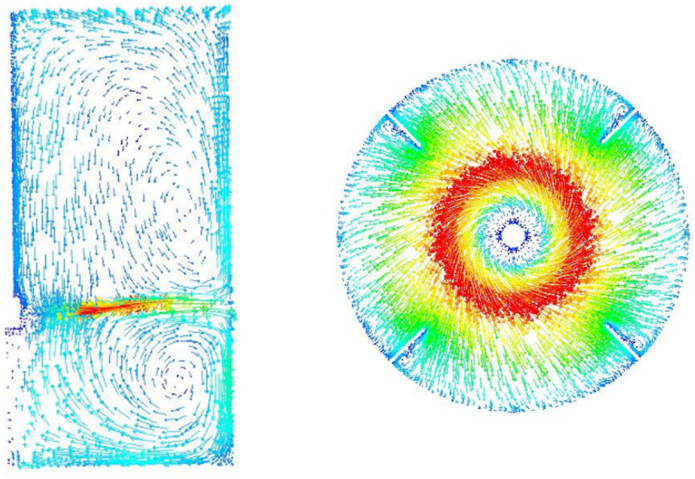

(**a**) (**b**)

Figure 15. Velocity magnitude field. (**a**) Side view of the tank. (**b**) Top view of the tank.

5.2. Influence of Different Geometric Configurations on the Fluid Dynamic Behavior and Mixture Time

In order to explore the developed model, some new theoretical recommendations were proposed for the influence of the dimensions of the baffles after applying constructal design [19,30]. The studied cases have the same dimensions for the tank previously shown in Figures 1 and 3. The only difference here is the shape of the baffles. The degree of freedom N_a (number of baffles) remains fixed ($N_a = 4$), while the degree of freedom L/B (corresponding to the size of the baffles) varies. Thus, seven different dimensions for the baffles were studied in addition to the unbaffled tank shown in Figure 4.

To evaluate the influence of the baffles on the flow, the average magnitude of the kinetic energy of turbulence in the system was investigated. It is considered that higher magnitudes of kinetic energy of turbulence represent configurations with more influence on fluid flow and the mixture process. From the results presented in Table 4 and Figure 16, it is clear that there is considerable variation in the flow when the geometry of the baffles is modified.

Table 4. Average magnitudes for the kinetic energy of turbulence in the system.

	L/B							
	Unbaffled	1	0.29	0.14	0.08	0.05	0.03	0.02
k (m²/s²)	0.041	0.028	0.021	0.018	0.017	0.020	0.023	0.026

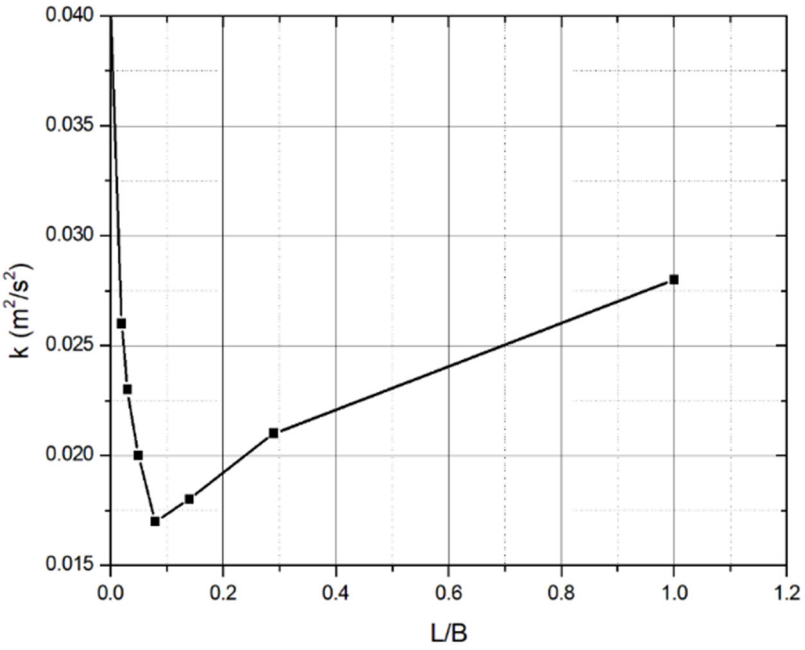

Figure 16. Effect of the ratio L/B on turbulence kinetic energy.

Based on the results presented in Table 4 and in Figures 16 and 17, it can be seen that the average turbulence kinetic energy is the highest for the unbaffled tank, and as the L/B ratio decreases, this average also decreases. This decrease occurs until $L/B = 0.08$, then the average turbulence kinetic energy starts to increase, i.e., the case where $L/B = 0.08$ presents the lowest value for the turbulence kinetic energy. It is worth mentioning that, in spite of high amounts of turbulence kinetic energy, the unbaffled tank and the lowest ratio of L/B presented obvious dead spot regions. For the unbaffled tank, they were at the periphery, whereas they were behind the baffles when $L/B = 0.02$. This behavior can impair the mixture in the whole domain. Figure 18 shows the fields of turbulent viscosity for the same configurations presented in Figure 17. The results for turbulent viscosity corroborate the

findings for turbulence kinetic energy, such that poor distribution of the turbulent viscosity occurred at the periphery of the unbaffled tank even though the highest magnitudes occurred in the central region. Moreover, the most distributed fields associated with high magnitudes of turbulent viscosity were noticed for the case when L/B = 1.0, while at the lowest value for L/B, large dead spots were caused by the intrusion of the baffles.

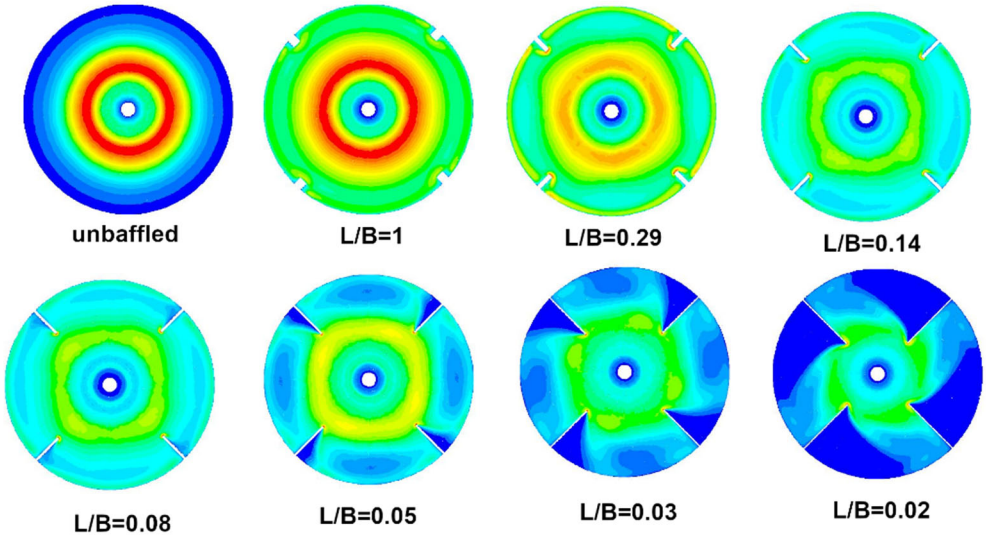

Figure 17. Distribution of the fields of turbulence kinetic energy in the baffled tank for different ratios of L/B compared to the unbaffled tank.

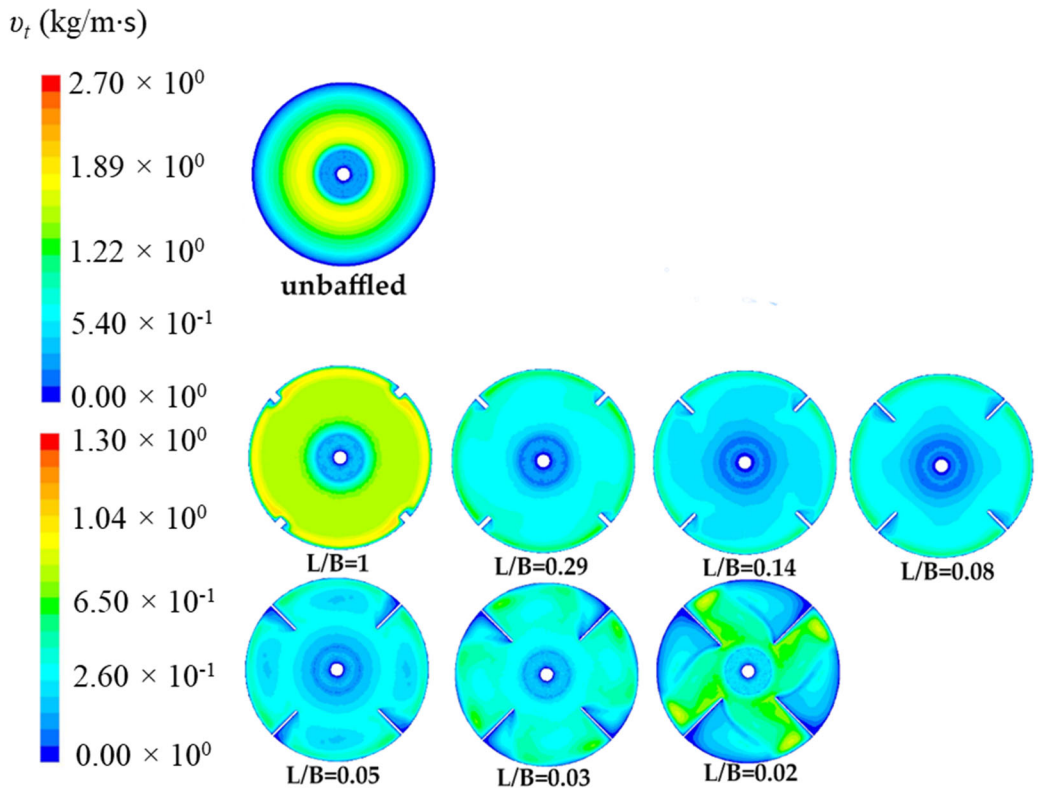

Figure 18. Distribution of the fields of turbulence viscosity in the baffled tank for different ratios of L/B compared to the unbaffled tank.

To evaluate the influence of the baffles on the mixture time, numerical simulations were performed using the species transport model. A tracer with the same fluid-dynamic

properties as the main fluid was inserted into the flow, as shown the Figure 19, and the standard deviation for the mass fraction of the tracer as a function of time was monitored in the tank domain.

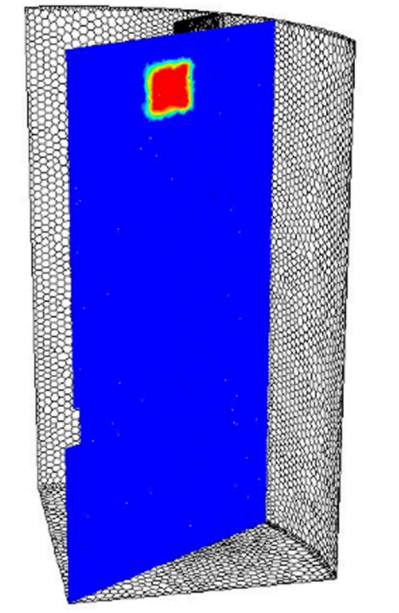

Figure 19. Illustration of the introduction of the tracer in the flow after achievement of the steady state.

Table 5 presents the maximum values for the tracer mass fraction as a function of time in the tank domain. The relative difference for the tracer mass fraction at each instant of time was calculated in order to obtain the instant at which the mass fraction changes were no longer relevant. Thus, when the values for the tracer mass fraction from one time step to the next showed a relative difference smaller than 5%, the variation was considered no longer relevant, and the tracer had achieved an equilibrium in the system.

Table 5. Maximum tracer mass fraction as a function of time in the tank domain.

	Time (s)	**Relative Difference (%)**
Unbaffled	5.0	4.82
L/B = 1.00	4.5	3.61
L/B = 0.29	4.5	1.18
L/B = 0.14	4.0	3.12
L/B = 0.08	4.5	3.01
L/B = 0.05	6.5	4.02
L/B = 0.03	5.0	3.95
L/B = 0.02	4.0	4.60

As shown in Table 5, the case that required the longest time, 6.5 s, to reach equilibrium in the system was when L/B = 0.05. The fastest time, 4.0 s, occurred when L/B = 0.14 and L/B = 0.02. Thus, all simulations modeling the behavior of the tracer in the system flow were run for a maximum time of t = 7.0 s. The result with the smallest standard deviation in the system was considered to represent the best mixture, as shown in Figure 20.

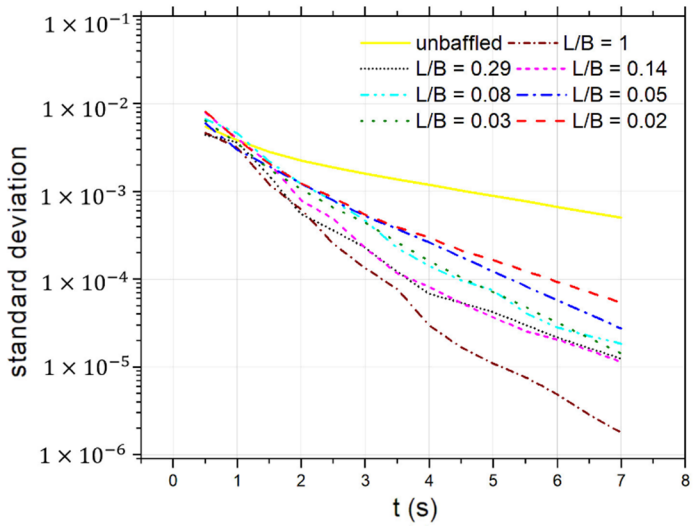

Figure 20. Standard deviation of the tracer mass fraction as a function of time for the different studied configurations.

It was observed that all cases initially had similarly large magnitudes for the standard deviation, since the tracer mass fraction kept changing as the system was being homogenized. For those cases that achieved equilibrium more quickly (L/B = 0.02 and L/B = 0.14), it was noted that the smallest standard deviation and consequently the best homogenization occurred when L/B = 0.14 (the baffles were shorter than the case with L/B = 0.02). However, the case that presented the smallest standard deviation of all was when L/B = 1.0, which only required 0.5 s longer for homogenization than those mentioned above. In this case, the baffles had the shortest length; moreover, performance was nearly two times better than the unbaffled configuration when minimization of standard deviation was used as the performance indicator. The largest standard deviation was seen in the case without baffles, and it required 5.0 s to reach equilibrium. Comparing the case without a baffle with the case where L/B = 1.0, it is easy to notice the influence of the baffles on the system, which changed the flow behavior as the length of the baffles increased towards the center of the tank. In Figure 21, the distribution of the tracer in the tank volume at t = 7.0 s is shown for all cases (L/B ratios).

Although the case without baffles had the largest turbulence kinetic energy, this kinetic energy had the highest concentration in the region closest to the impeller without being distributed to the rest of the tank, so the standard deviation for this case was also the highest. For the case when L/B = 1.0, the presence of baffles assisted in the distribution of turbulence kinetic energy in the tank domain, increasing the homogenization capacity of the system and producing the smallest value for the tracer standard deviation. As the baffles grow in length in the tank domain (until they reach L/B = 0.08), the turbulence kinetic energy decreases, and homogenization of the system is more difficult due to the generation of large regions of stagnation in the tank domain. In contrast, from L/B = 0.05 to L/B = 0.02, the turbulence kinetic energy begins to increase. However, this increase does not assist in homogenization of the system since the baffles are unable to distribute the turbulence kinetic energy and high concentrations develop close to the impeller. This behavior occurs because the baffles have become so long that the flow behaves as if it were in a tank without baffles but with a smaller radius (from the center to the tip of each baffle). Thus, from the analysis carried out, it can be concluded that the case with the best efficiency in terms of time and homogenization of the system was when L/B = 1.0. Figure 22 shows the evolution over time of tracer distribution for the case where L/B = 1.0.

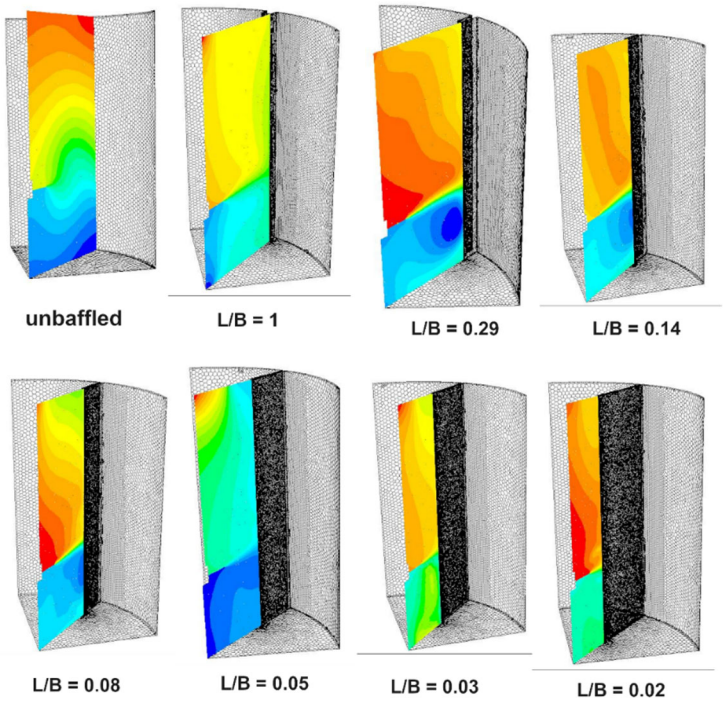

Figure 21. Distribution of the tracer in the tank volume at t = 7.0 s for all cases.

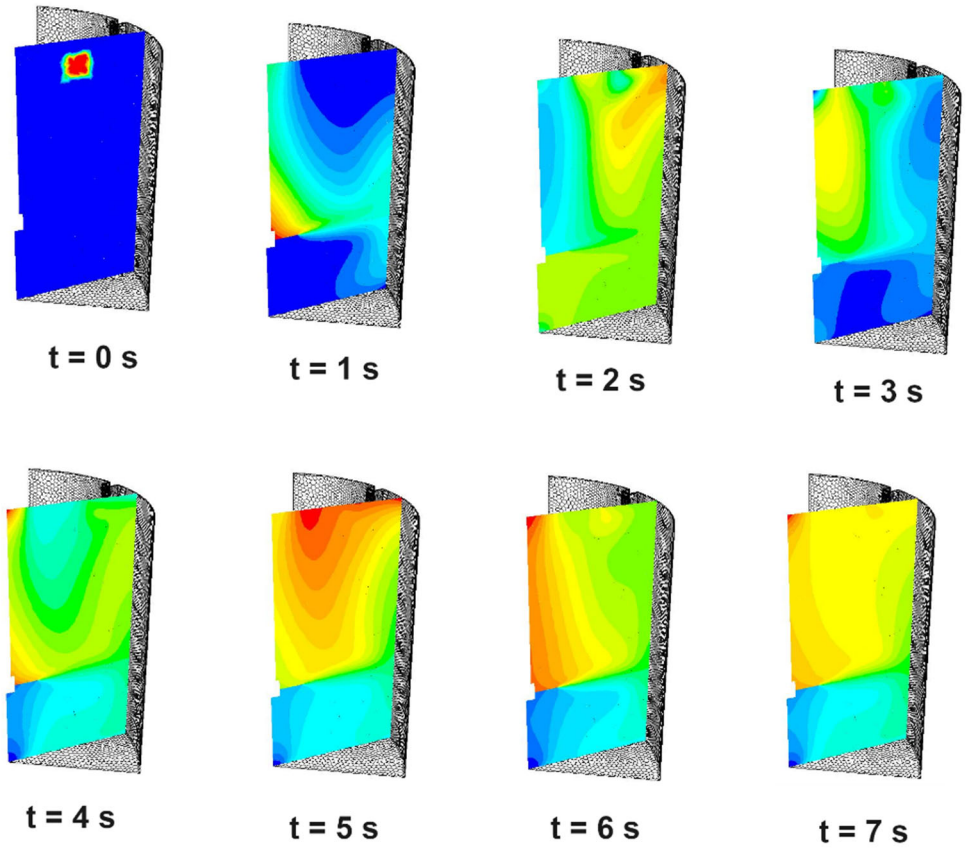

Figure 22. Evolution over time of the tracer distribution in the case where L/B = 1.0.

It is worth mentioning that the optimal case is the one that equilibrates the distribution of dead spots in the tank domain. In comparison with the unbaffled case, the optimal configuration prevents the concentration of dead spots in the peripheral region of the tank; and in comparison with the other extreme (L/B = 0.02), it does not generate large

regions of dead spots behind the baffles. Therefore, the results are in agreement with the constructal principle of "optimal distribution of imperfections".

6. Conclusions

The present numerical work presents the development of strategies for numerical simulation of turbulent flows in stirred tanks with the lowest computational effort possible. A computational model based on a momentum source imposed by a UDF was compared with another model based on the use of a sliding mesh, which required a much greater computational effort. The momentum source model allowed the geometric configuration of rectangular baffles to be investigated by means of the constructal design method with the goal of obtaining new recommendations on the effects of the configuration of the baffles on the mixture and mixing time for flows into a stirred tank. The influence of the geometric configuration of the baffles on turbulence kinetic energy and distribution of a tracer in the tank domain were also considered.

The momentum source model is recommended for future investigations of geometric configurations of baffles in stirred tanks since it generated results for velocity fields similar to those previously predicted experimentally and numerically in the literature [11,29] and those obtained with a sliding mesh with a computational cost of only 2% of that required by the sliding mesh model. In addition, the momentum source model provides advantages in relation to its ability to generate a simpler computational domain, of being able to simulate a partial domain and providing greater mesh refinement with less computational effort.

For the study of the mixture homogenization in the tank, a species transport model without chemical reactions was used. The results indicated that the case without baffles produced the highest turbulence kinetic energy. However, the unbaffled case produced a mixture that was poorly distributed along the tank domain.

The results also demonstrated the importance of geometrical investigation for this kind of problem and the applicability of the constructal design method. The best performance related to the mixture of fluid flow along the domain was obtained for the case $(L/B)_o = 1.0$, which provided a mixture performance (given by the standard deviation of mixture in the domain) that was two times better than the unbaffled case. The optimal configuration was the one that best equilibrated the distribution of dead spots of turbulent flow in the domain, and this behavior is in agreement with the constructal principle of "optimal distribution of imperfections".

In the future, other flow conditions will be investigated (since the Reynolds number was imposed for the current problem), the number of baffles will be varied (N_a = 2, 6 and 8) and other geometrical configurations for the baffles (circular and ellipsoidal) will be explored.

Author Contributions: Conceptualization, L.L.S., J.A.A.O.J., E.D.d.S. and M.M.G.; methodology, L.L.S., J.A.A.O.J., E.D.d.S. and M.M.G.; formal analysis, L.L.S., C.B., E.D.d.S. and M.M.G.; investigation, L.L.S. and R.d.R.C.; resources, C.B., J.A.A.O.J., E.D.d.S. and M.M.G.; data curation, L.L.S., R.d.R.C. and M.M.G.; writing—original draft preparation, L.L.S., E.D.d.S. and M.M.G.; writing—review and editing, C.B., E.D.d.S. and M.M.G.; visualization, L.L.S., C.B., E.D.d.S. and M.M.G.; supervision, E.D.d.S. and M.M.G.; project administration, C.B., E.D.d.S. and M.M.G.; funding acquisition, C.B., E.D.d.S. and M.M.G. All authors have read and agreed to the published version of the manuscript.

Funding: This research was supported by CAPES (Coordination for the Improvement of Higher Educational Personal) doctorate research scholarship (Finance Code 001). Research grant CNPq (National Counsel of Technological and Scientific Development—Brasília, DF, Brazil) (Process: 308396/2021-9). Cesare Biserni is sponsored by the Italian Ministry for Education, University and Research.

Institutional Review Board Statement: Not applicable.

Informed Consent Statement: Not applicable.

Data Availability Statement: The data to support the findings of this study are available from the authors upon request.

Acknowledgments: The authors thank the Federal Education Science and Technology Institute of Rio Grande do Sul (IFRS), Federal University of Rio Grande (FURG), and University of Bologna (UNIBO) for support in the research. Elizaldo Domingues dos Santos thanks CNPq for research grant (Process: 308396/2021-9) and Cesare Biserni thanks the Italian Ministry for Education, University and Research.

Conflicts of Interest: The authors declare no conflict of interest.

References

1. Hartmann, H.; Derksen, J.J.; van den Akker, H.E.A. Mixing Times in a Turbulent Stirred Tank by Means of LES. *AIChE J.* **2006**, *52*, 3696–3706. https://doi.org/10.1002/aic.10997.
2. Foukrach, M.; Bouzit, M.; Ameur, H.; Kamla, Y. Influence of the Vessel Shape on the Performance of a Mechanically Agitated System. *Chem. Pap.* **2019**, *73*, 469–480. https://doi.org/10.1007/s11696-018-0606-4.
3. Till, Z.; Molnár, B.; Egedy, A.; Varga, T. CFD Based Qualification of Mixing Efficiency of Stirred Vessels. *Period. Polytech. Chem. Eng.* **2018**, *63*, 226–238. https://doi.org/10.3311/PPch.12245.
4. Yang, F.; Zhou, S.; Wang, G. Detached Eddy Simulation of the Liquid Mixing in Stirred Tanks. *Comput. Fluids* **2012**, *64*, 74–82. https://doi.org/10.1016/j.compfluid.2012.05.005.
5. Paul, E.L., Atiemo-Obeng, V.A., Kresta, S.M. (Eds.) *Handbook of Industrial Mixing: Science and Practice*; Wiley-Interscience: Hoboken, NJ, USA, 2004; ISBN 978-0-471-26919-9.
6. Pukkella, A.K.; Vysyaraju, R.; Tammishetti, V.; Rai, B.; Subramanian, S. Improved Mixing of Solid Suspensions in Stirred Tanks with Interface Baffles: CFD Simulation and Experimental Validation. *Chem. Eng. J.* **2019**, *358*, 621–633. https://doi.org/10.1016/j.cej.2018.10.020.
7. Harnby, N.; Edwards, M.F.; Nienow, A.W.; (Eds.) *Mixing in the Process Industries*, 2nd ed.; pbk. ed.; Butterworth-Heinemann: Oxford, UK ; Boston, MA, USA, 1997; ISBN 978-0-7506-3760-2.
8. Başbuğ, S.; Papadakis, G.; Vassilicos, J.C. Reduced Mixing Time in Stirred Vessels by Means of Irregular Impellers. *Phys. Rev. Fluids* **2018**, *3*. https://doi.org/10.1103/PhysRevFluids.3.084502.
9. Li, L.; Xiang, K.; Xiang, B. Numerical Simulation of Transient Power Consumption Characteristics in an Unbaffled Stirred Tank. *Chem. Pap.* **2020**, *74*, 2849–2859. https://doi.org/10.1007/s11696-020-01115-3.
10. Li, L.; Xu, B. CFD Simulation of Local and Global Mixing Time in an Agitated Tank. *Chin. J. Mech. Eng.* **2017**, *30*, 118–126. https://doi.org/10.3901/CJME.2016.1107.129.
11. Javed, K.H.; Mahmud, T.; Zhu, J.M. Numerical Simulation of Turbulent Batch Mixing in a Vessel Agitated by a Rushton Turbine. *Chem. Eng. Process. Process Intensif.* **2006**, *45*, 99–112. https://doi.org/10.1016/j.cep.2005.06.006.
12. Yeoh, S.L.; Papadakis, G.; Yianneskis, M. Determination of Mixing Time and Degree of Homogeneity in Stirred Vessels with Large Eddy Simulation. *Chem. Eng. Sci.* **2005**, *60*, 2293–2302. https://doi.org/10.1016/j.ces.2004.10.048.
13. Karadimou, D.P.; Papadopoulos, P.A.; Markatos, N.C. Mathematical modelling and numerical simulation of two-phase gas-liquid flows in stirred-tank reactors. *J. King Saud Univ.* **2019**, *31*, 33–41. https://doi.org/10.1016/j.jksus.2017.05.015.
14. Yapici, K.; Karasozen, B.; Schäfer, M.; Uludag, Y. Numerical Investigation of the Effect of the Rushton Type Turbine Design Factors on Agitated Tank Flow Characteristics. *Chem. Eng. Process. Process Intensif.* **2008**, *47*, 1340–1349. https://doi.org/10.1016/j.cep.2007.05.002.
15. Gu, D.; Cheng, C.; Liu, Z.; Wang, Y. Numerical Simulation of Solid-Liquid Mixing Characteristics in a Stirred Tank with Fractal Impellers. *Adv. Powder Technol.* **2019**, *30*, 2126–2138. https://doi.org/10.1016/j.apt.2019.06.028.
16. Başbuğ, S.; Papadakis, G.; Vassilicos, J.C. Reduced Power Consumption in Stirred Vessels by Means of Fractal Impellers. *AIChE J.* **2018**, *64*, 1485–1499. https://doi.org/10.1002/aic.16096.
17. Foukrach, M.; Bouzit, M.; Ameur, H.; Kamla, Y. Effect of Agitator's Types on the Hydrodynamic Flow in an Agitated Tank. *Chin. J. Mech. Eng.* **2020**, *33*, 37. https://doi.org/10.1186/s10033-020-00454-2.
18. Tamburini, A.; Gagliano, G.; Micale, G.; Brucato, A.; Scargiali, F.; Ciofalo, M. Direct Numerical Simulations of Creeping to Early Turbulent Flow in Unbaffled and Baffled Stirred Tanks. *Chem. Eng. Sci.* **2018**, *192*, 161–175. https://doi.org/10.1016/j.ces.2018.07.023.
19. Bejan, A.; Lorente, S. *Design with Constructal Theory*; John Wiley & Sons: Hoboken, NJ, USA, 2008; ISBN 978-0-471-99816-7.
20. Bejan, A. *Freedom and Evolution: Hierarchy in Nature, Society and Science*; Springer International Publishing: Cham, Switzerland, 2020; ISBN 978-3-030-34008-7.
21. Bejan, A.; Zane, J.P. *Design in Nature: How the Constructal Law Governs Evolution in Biology, Physics, Technology, and Social Organization*; Anchor Books: New York, 2012; ISBN 978-0-385-53462-8.
22. Bejan, A. Thermodynamics Today. *Energy* **2018**, *160*, 1208–1219. https://doi.org/10.1016/j.energy.2018.07.092.
23. Magalhães, G.M.C.; Fragassa, C.; Lemos, R.d.L.; Isoldi, L.A.; Amico, S.C.; Rocha, L.A.O.; Souza, J.A.; dos Santos, E.D. Numerical Analysis of the Influence of Empty Channels Design on Performance of Resin Flow in a Porous Plate. *Appl. Sci.* **2020**, *10*, 4054. https://doi.org/10.3390/app10114054.

24. ANSYS. *ANSYS Fluent User's Guide*; Ansys Inc., New York, NY, USA, 2009.
25. Versteeg, H.K.; Malalasekera, W. *An Introduction to Computational Fluid Dynamics: The Finite Volume Method*; Nachdr.; Pearson/Prentice Hall: Harlow, UK, 2005; ISBN 978-0-582-21884-0.
26. Schlichting, H.; Gersten, K. *Boundary-Layer Theory*, 8 rev.enl. ed.; Physics and astronomy online library; corr. print.; Springer: Berlin, Germany, 2003; ISBN 978-3-540-66270-9.
27. Launder, B.E.; Spalding, D.B. The Numerical Computation of Turbulent Flows. In *Numerical Prediction of Flow, Heat Transfer, Turbulence and Combustion*; Elsevier: Amsterdam, The Netherlands, 1983; pp. 96–116, ISBN 978-0-08-030937-8.
28. Wilcox, D.C. *Turbulence Modeling for CFD*, 3rd ed.; DCW Industries: La Cãnada, CA, USA, 2006; ISBN 978-1-928729-08-2.
29. Huang, W.; Li, K. CFD Simulation of Flows in Stirred Tank Reactors through Prediction of Momentum Source. In *Nuclear Reactor Thermal Hydraulics and Other Applications*; Guillen, D., Ed.; InTech: London, UK, 2013; ISBN 978-953-51-0987-7.
30. dos Santos, E.D.; Isoldi, L.A.; Gomes, M. das N.; Rocha, L.A.O. The Constructal Design Applied to Renewable Energy Systems. In *Sustainable Energy Technologies*; Rincón-Mejía, E., de las Heras, A., Eds.; CRC Press: Boca Raton, FL, USA, 2017; pp. 45–62, ISBN 978-1-315-26997-9.
31. Gonzales, G.V.; Lorenzini, G.; Isoldi, L.A.; Rocha, L.A.O.; dos Santos, E.D.; Neto, A.J.S. Constructal Design and Simulated Annealing Applied to the Geometric Optimization of an Isothermal Double T-Shaped Cavity. *Int. J. Heat Mass Transf.* **2021**, *174*, 121268. https://doi.org/10.1016/j.ijheatmasstransfer.2021.121268.
32. *ASME Standard for Verification and Validation in Computacional Fluid Dynamics and Heat Transfer*; The American Society of Mechanical Engineers (ASME): New York, NY, USA, 2009.
33. Roache, P.J. *Verification and Validation in Computational Science and Engineering*; Hermosa Publishers: Albuquerque, NM, USA, 1998; ISBN 978-0913478080.
34. Martins, J.C.; Fragassa, C.; Goulart, M.M.; Dos Santos, E.D.; Isoldi, L.A.; Gomes, M.N.; Rocha, L.A.O. Constructal Design of an Overtopping Wave Energy Converter Incorporated in a Breakwater. *J. Mar. Sci. Eng.* **2022**, *10*, 471–28. https://doi.org/10.3390/jmse10040471.